# Occam and Bostick 1-D inversion of magnetotelluric soundings in the Chicxulub Impact Crater, Yucatán, Mexico

Omar Delgado-Rodríguez[1,*], Oscar Campos-Enríquez[1], Jaime Urrutia-Fucugauchi[1] and Jorge A. Arzate[2]

[1] *Laboratorio de Paleomagnetismo y Geofísica Nuclear, Instituto de Geofísica, UNAM, México, D. F., MÉXICO*

[2] *Unidad de Investigación en Ciencias de la Tierra, Instituto de Geofísica, UNAM, Campus Juriquilla, Querétaro, MÉXICO*

[*] *Now at Instituto Mexicano del Petróleo, México, D. F., MÉXICO*

### RESUMEN

En este estudio se presenta la investigación realizada en el sector sureste del cráter de Chicxulub mediante la aplicación del método de Sondeo Magnetotelúrico (MT). El perfil MT analizado consta de diez sondeos MT distribuidos a lo largo de 92.5 km en la dirección radial SE-NW, tomando como centro el puerto de Chicxulub. En general, los sondeos MT exponen un medio uni-dimensional, con magnitudes de Tipper menores de 0.2. Tres sondeos contiguos presentan una ligera anisotropía y los mayores valores de Tipper para períodos largos. El comportamiento de la resistividad en estos sondeos para períodos mayores de 16 s define el límite estructural del cráter, implicando para la estructura de impacto de Chicxulub un diámetro aproximado de 200 km. Modelos unidimensionales, utilizando los esquemas de inversión de Bostick y Occam, fueron utilizados para investigar la estructura del cráter. Resistividades superiores e inferiores a 150 ohm-m caracterizan el medio fuera y dentro del anillo de cenotes, respectivamente.

PALABRAS CLAVE: Sondeo magnetotelúrico, inversión 1-D, anillo de cenotes, cráter de impacto de Chicxulub.

### ABSTRACT

The subsurface structure of the southeastern sector of the Chicxulub impact crater is investigated by ten magnetotelluric (MT) soundings distributed along a radial 92.5 km profile oriented SE-NW from the approximate center of the crater at Chicxulub Puerto. In general, MT soundings are one-dimensional, with Tipper magnitudes well below 0.2. Three contiguous soundings present a slight anisotropy and the largest Tipper values at frequencies lower than 0.06 Hz. This defines the structural rim of the crater at the cenote ring zone. Resistivities are respectively higher and lower than 150 ohm-m outside and inside the cenote ring. One-dimensional modeling using Bostick and Occam inversion yields similar geoelectrical models and is justified for most sites as a first approximation.

KEY WORDS: Magnetotelluric soundings, 1-D inversion, cenote ring, Chicxulub impact crater.

## INTRODUCTION

For more than a decade geological and geophysical studies have been carried out on the subsurface structure of the Chicxulub impact crater, in the northwestern Yucatán peninsula (Figure 1). Penfield and Camargo (1981) proposed the presence of an impact crater buried beneath a thick cover of Tertiary carbonate sediments. It took several years to link the Chicxulub crater with an impact at the Cretaceous/Tertiary (K/T) boundary (Hildebrand *et al.*, 1991; Sharpton *et al.*, 1992). Following the study by Alvarez *et al.* (1980), a world-wide search was launched to locate the impact site. Several candidate craters were considered before the search concentrated on the Gulf of Mexico and Caribbean region (Bourgeois *et al.*, 1988).

Initial studies of the structure based on gravity and mag-netic data and on core samples from Pemex proposed crater diameters ranging from 180 to 300 km and complex crater models with a peak-ring or multi-ring structure (e.g., Hildebrand *et al.,* 1991; Sharpton *et al.,* 1993; Pilkington *et al.,* 1994; Espíndola *et al.,* 1995; Hildebrand *et al.,* 1998). A drilling program by UNAM included eight boreholes in the southern sector of the crater (Urrutia-Fucugauchi *et al.,* 1996). Nearly complete lithological columns are now available for this sector of the crater, for detailed geometrical modeling of the impact breccia distribution (Rebolledo-Vieyra *et al.,* 2000). Marine seismic reflection profiles and onshore wide-angle seismic profiles across the crater support a 180-210 km multi-ring impact basin (Morgan *et al.,* 1997). Further analyses of the seismic data have resulted in refinements of the crater structure and the size and nature of the crater inner, peak and outer rings (e.g., Morgan and Warner, 1999; Snyder *et al.,* 1999).
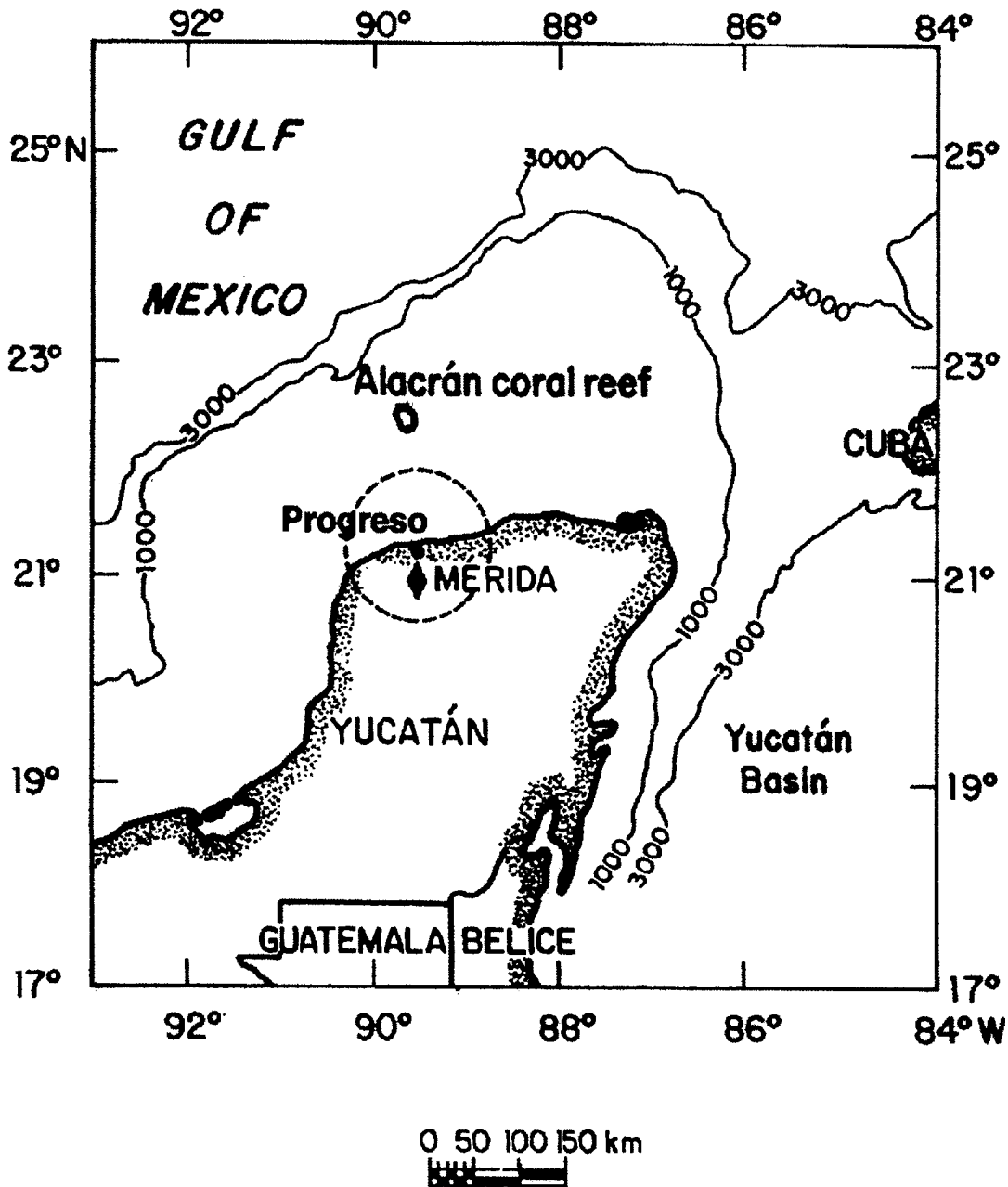
Fig. 1. Study area. The concentric circle approximately indicate the impact structure. PThe cities of Mérida and Progreso are located in the circle.

The Chicxulub Scientific Drilling Project (CSDP) has selected as initial target zone a sector SE of the Yucatan-6 Pemex well, inside the cenote ring. For this purpose detailed studies of this sector of the crater including high-resolution geophysical surveys and shallow drilling are required.

In this paper we present a modeling and initial interpretation of an one-dimensional (1-D) magnetotelluric (MT) inversion of ten soundings along a SE-NW 92.5 km long profile (B-B' profile) normal to the cenote ring (Figure 2).

We use Bostick and Occam (Constable *et al.,* 1987) inversion algorithms for modeling the MT data. The MT sounding profile is located to the east of the CSDP target zone.

## MAGNETOTELLURIC SURVEY

Gravity, magnetic and seismic surveys have been used to study impact structures (Pilkington and Grieve, 1992). Geoelectrical methods have also been applied to investi-
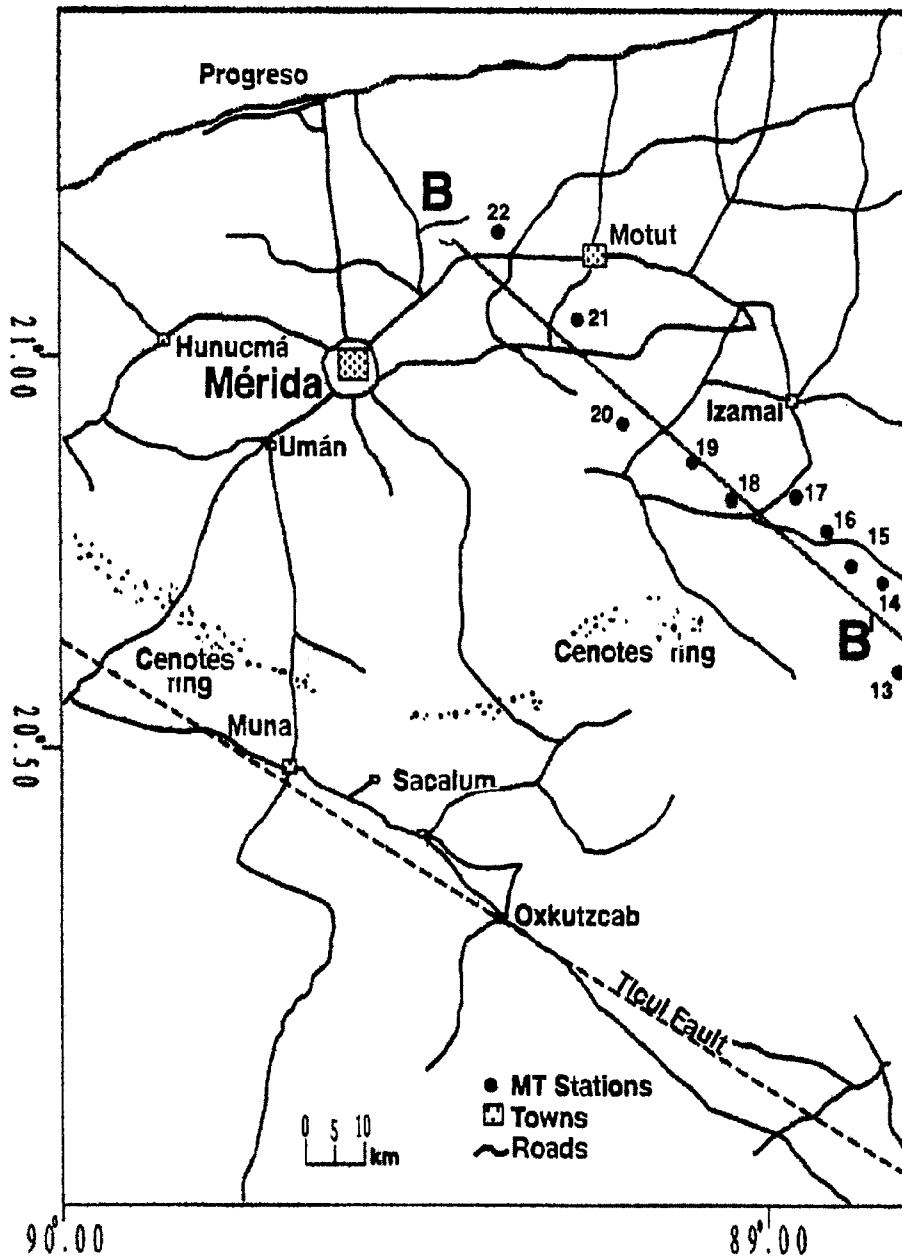
Fig. 2. Location of the magnetotelluric sounding stations in the study area.

gate impact craters. Electrical resistivity data have proved useful in mapping the extent of authigenic brecciation (Henkel, 1992). Electromagnetic methods have been developed for shallow and deep crustal investigations. A particularly powerful method is the MT sounding method (Cagniard, 1953).

We recorded the three components hx, hy, and hz of the magnetic field and the horizontal components ex and ey of the electric field. Here, **x** points to the geomagnetic north,

**y** points to the east, and **z** points vertically downwards. Cross-spectra are calculated to determine the impedance tensor (Z), which conveys information about the subsurface (Vozoff, 1989).

The study comprising 22 MT soundings was conducted in the central and southern region of the impact crater (Campos-Enríquez *et al.,* 1997). Ten magnetotelluric soundings were obtained along a SE-NW 92.5 km long profile (B-B'), normal to cenote ring where the 200-210 km limit of the

273

crater structure is assumed to be located (Figure 2). The profile is located to the SE of Merida City.

We used two Phoenix V-5 MT instruments operating on a remote basis. Observations cover the range between a frequency of 384 Hz and a period of 1820 s.

The profile is inland to reduce its coast effects on MT observations. Parkinson (1959) described the coast effect in electromagnetic observations as a result of the influence of the high electric conductivity of seawater (Kellet *et al.,* 1991). The influence of a highly conductive body may affect geomagnetic measurements in a way that suggests a spurious presence of a conductive stratum in the interpretation of resistivity $\rho(\omega)$ and phase $\phi(\omega)$ curves. In addition, it can mask the real effect of an anomalous conductive body, which could be possibly associated with the Chicxulub impact crater. A recent quantitative evaluation of the coast effect in the Yucatán peninsula suggests that the effect is negligible in the crater region (Delgado *et al.,* 2001).

The impedance tensor for the MT stations was rotated -45°, establishing xy as TM mode and yx as TE mode, thus current flows across and along the crater boundary. Radial distances are referred to the center of the impact structure at Chicxulub puerto, about 7 km to the E of Puerto Progreso (Figure 2). A preliminary evaluation of MT data was presented in Campos-Enríquez *et al.* (1997), based on a Bostick inversion of the xy apparent resistivity and phase curves. High resistivities were observed beneath the second group of soundings, south of the cenote ring. Inside the cenote ring, resistivity decreased smoothly up to sounding 20 and increased again toward the end of the profile. The high values towards the crater center beneath sounding 22 may be due to the central structural uplift inferred from gravity and magnetic anomalies.

In this study, each pair of resistivity and phase curves $\rho_{axy}(\omega)$, $\phi_{xy}(\omega)$ and $\rho_{ayx}(\omega)$, $\phi_{yx}(\omega)$ is interpreted in order to calculate two independent geoelectric models. The Bostick (1977) and Occam (Constable *et al.,* 1987) inversion schemes have been used in this study.

## DATA ANALYSIS

Figure 3 shows the variance of the phase and resistivity observations. Low variances (SD < 5%) are observed for the electrical resistivity (Figures 3a and 3b), except at MT sounding 21, which exceeds 45%.

Figures 3c and 3d show the variance of the observed phases. Again the peak values are observed around sounding 21. High variances (SD > 45%) are observed for MT soundings 16, 18 and 20, contrasting with electrical resistivity vari-

ance (Figures 3a and 3b). These results suggest that phase is more sensitive to noise than resistivity, especially at low frequency.

Because of the high variance values at sounding 21, observations at this sounding for frequencies below 1 Hz were discarded. Sounding 21 was only used to study the shallow part of the area.

Figure 4 shows the apparent resistivity and phase sections. Good agreement between the values of $\rho_{axy}(\omega)$ and $\rho_{ayx}(\omega)$ (Figures 4a and 4b) was observed at nearly all stations, except at MT sounding 20 where (for frequencies less than 0.4 Hz) the increase in $\rho_{axy}(\omega)$ (Figure 4a) is not present in $\rho_{ayx}(\omega)$ (Figure 4b).

At MT soundings 13, 14 and 15, the joint increase in apparent resistivity may indicate the presence of the outer ring south of the cenote ring (Figure 2).

The Bouguer anomaly map shows the location of the MT soundings (Figure 6). Note three zones along the MT profile as follows.

Zone I of peak gravity values includes MT soundings 13, 14 and 15. This zone is outside of the cenote ring and little fractured or unfractured carbonated rocks are expected.

Zone II of low gravity values includes the MT soundings 18, 19, 20, and 21. Highly fractured rocks (breccias), constituting the main component of the crater filling are expected.

Between zones I and II we find a steep gravity gradient. This transition region includes the cenote ring and MT soundings 16 and 17.

Zone III is associated with the central gravity maximum suggesting a structural high typical of complex impact craters. The impact melt sheet and melt breccia contribute to higher gravity values. In this zone there are no MT soundings, but sounding 21 is in the transition zone (high gravity gradient) between zones II and III.

The phase (Figures 4c and 4d) also present a great similarity, except in the sections mentioned above.

Tipper (T) and Skew (S) sections were computed (Figure 5). Low values of Tipper (T < 0.2) are indicative of a 1-D structure, while higher values (T ≥ 0.2) suggest effects of 2-D or 3-D structures. High Skew (k ≥ 0.4) indicate the presence of 3-D structures. In Figure 5a, the highest values
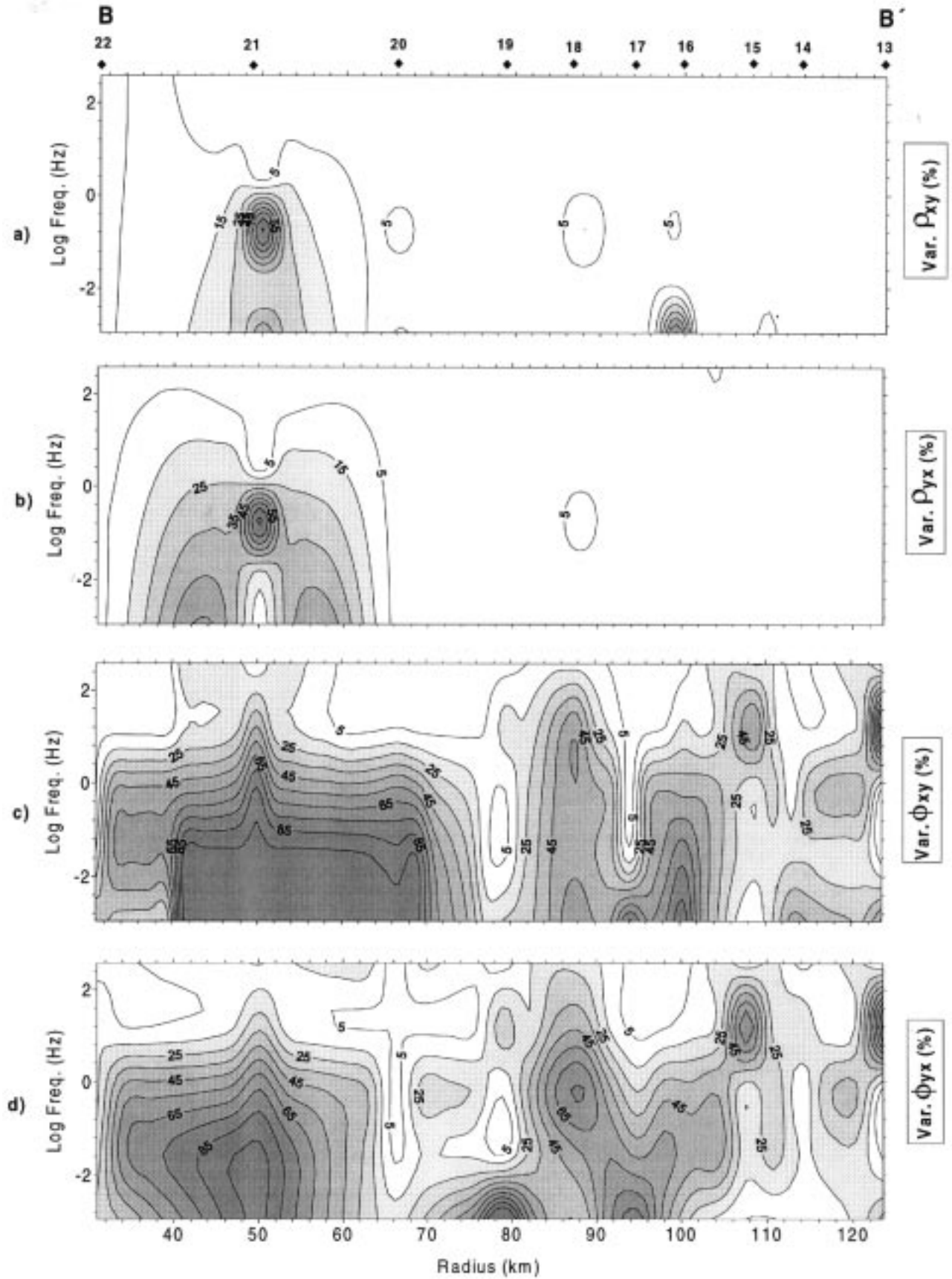
Fig. 3. Variance sections in %. a) xy apparent resisitivity, b) yx apparent resistivity, c) xy Phase and d) yx Phase.
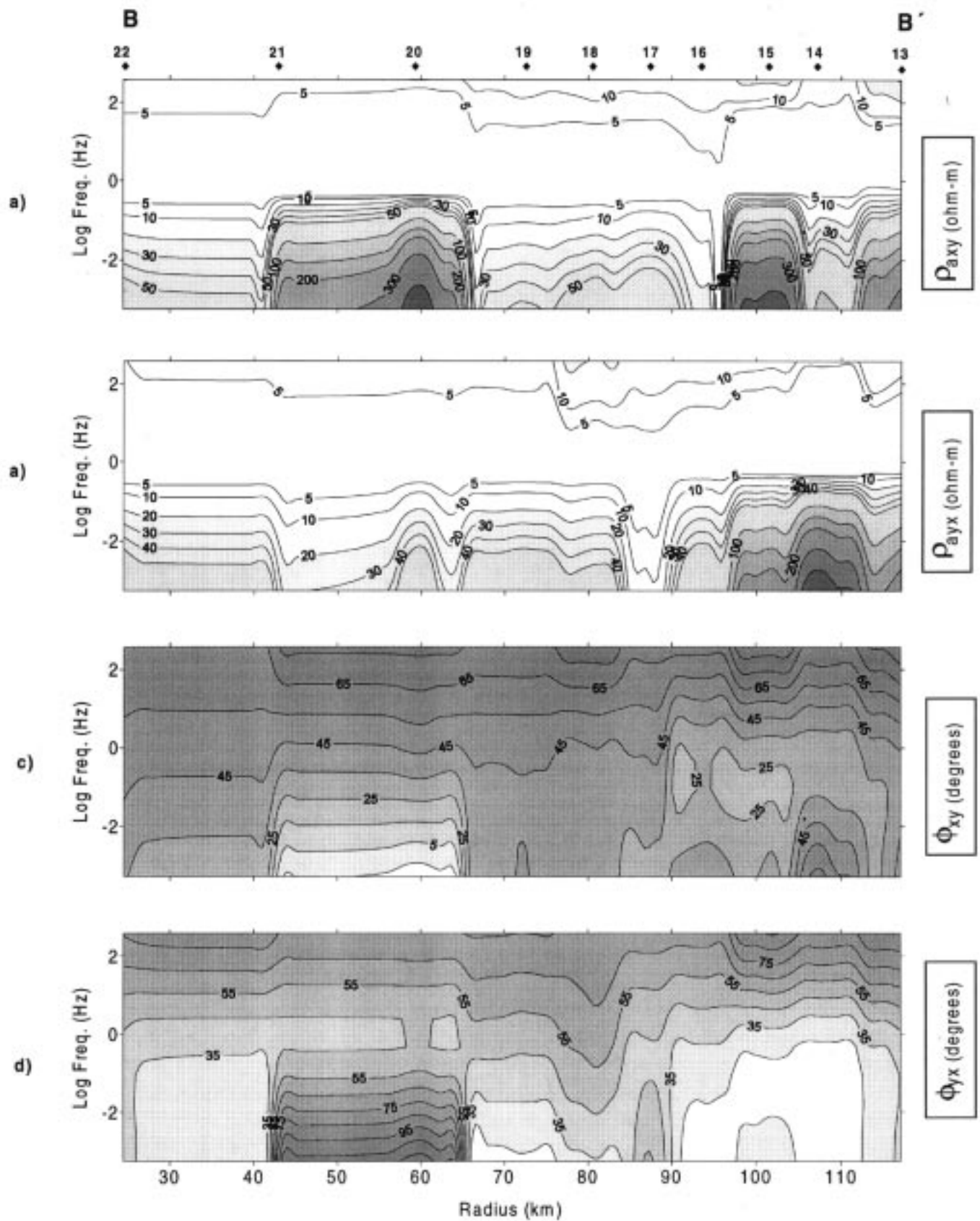
Fig. 4. Observed pseudosections. a) xy apparent resistivity, b) yx apparent resistivity, c) xy Phase  and d) yx Phase.

of Tipper (Tip > 0.4) are observed in soundings 13, 14 and 15 for frequencies below 0.06 Hz.

The increase in Tipper magnitude could indicate the presence of a local strike related to the outer ring of the impact structure. Figure 5b suggests a 3-D distortion at sounding 16 for frequencies less than 0.3 Hz, and for sounding 20 at frequencies less than 0.01 Hz.

In conclusion, soundings 13, 14 and 15, for periods larger than 16 s, define a local strike, while sounding 20 at lower frequencies indicates the existence of a geoelectric contrast that introduces 3-D distortion.

On the whole, apparent resistivity, phase, Tipper and Skew sections agree with 1-D modeling, and justify the use of 1-D inversion algorithms such as those of Bostick and Occam.

## BOSTICK INVERSION

This heuristic inversion scheme generates a continuous or near-continuous resistivity distribution versus depth (Bostick, 1977). In this study, we estimated the resistivity by means of the apparent resistivity, and the observed phase by

$$\rho(z) = \rho_a(\omega)\left(\frac{\pi}{2\phi(\omega)} - 1\right), (1)$$

$$z = \left(\frac{\rho_a(\omega)}{\mu\omega}\right)^{\frac{1}{2}}, \qquad (2)$$

where $z$ is the nominal depth corresponding to the skin depth of a half-space of apparent resistivity $\rho_a$ and frequency $\omega$.
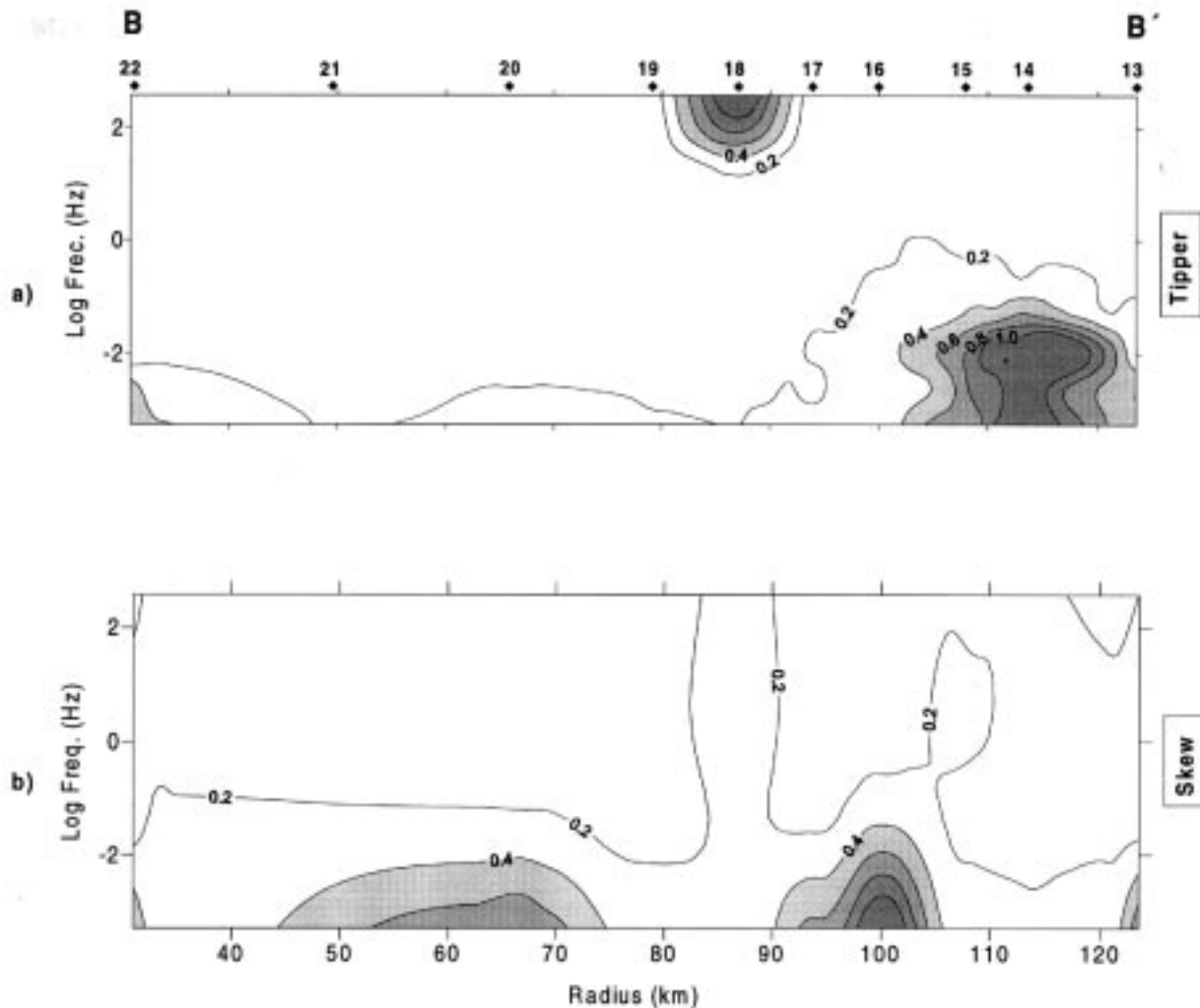


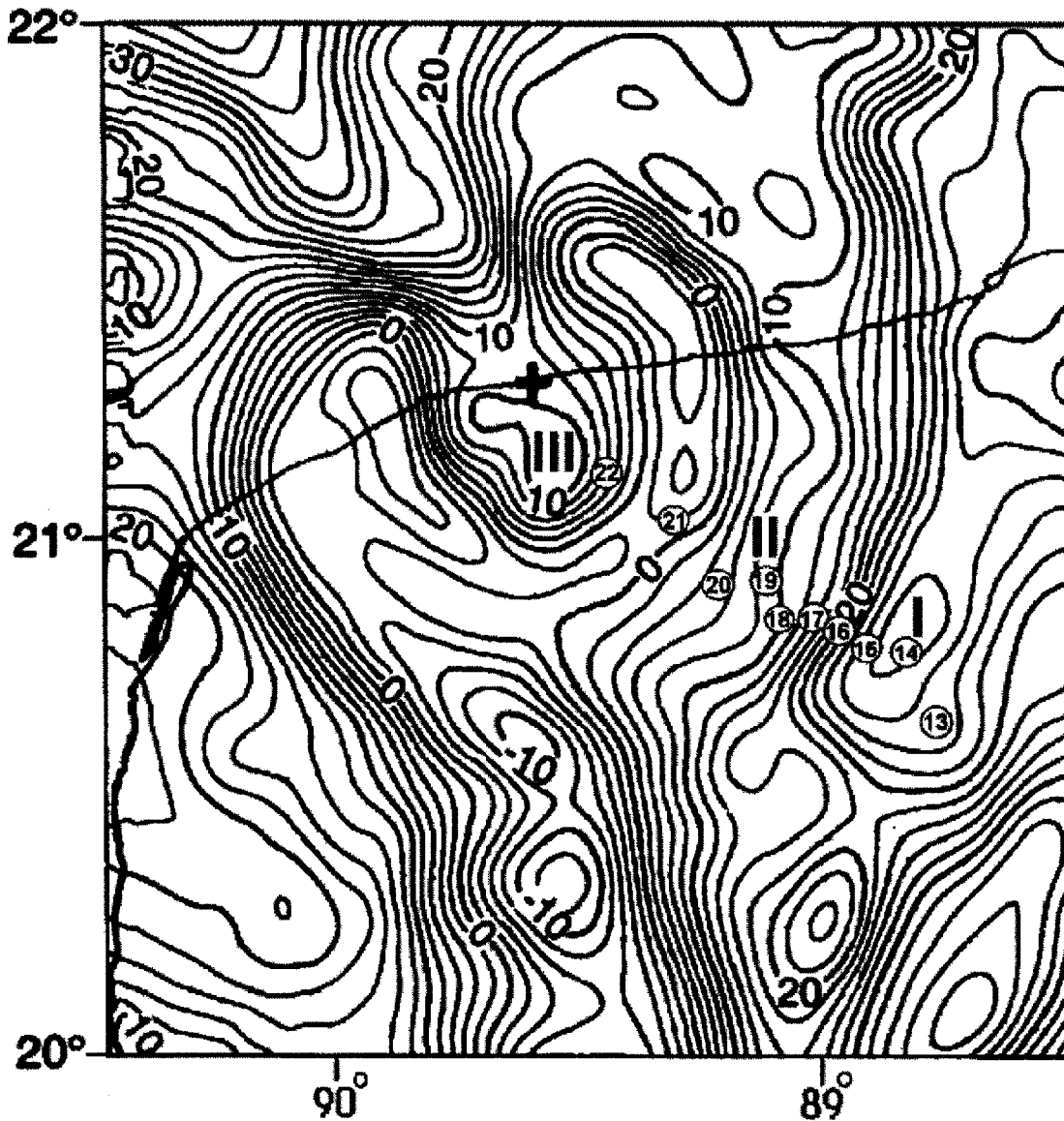Fig. 5. Distortion analysis. a) Tipper section, b) Skew section.

Fig. 6. Bouguer anomaly map. The values on the map are given in mgals. The location of MT soundings is indicated by encircled number.

In Figures 7a and 7b, the $\rho_{xy}$ and $\rho_{yx}$ models for the Bostick inversion are shown. Similar results are found for both models. Dominant resistivity values $\rho(z) > 150$ ohm-m at soundings 13, 14 and 15 (zone I, Figure 6), indicate the basin limits, while resistivity values of less than 150 ohm-m set off the filling of the crater from the rest of the MT soundings in zone II (Campos-Enríquez *et al.,* 1997).

The $\rho_{yx}$ section shows the outer ring between MT soundings 15 and 16 more sharply. Note, a zone of minimum values of $\rho_{yx}(z)$ between soundings 16 to 18, that is not clearly found in the $\rho_{xy}$ model. This zone coincides with the external ring of minimum gravity values from the Bouguer anomalies map (Figure 6). Our result agrees with a structural fea-

ture around sounding 16, with a maximum diameter for the crater of about 200 km.

In the $\rho_{xy}$ as well as in the $\rho_{yx}$ model, an increment of the resistivity with depth is observed near sounding 22. Keeping in mind the postulated central structural high, this might contain the denser and less fractured materials.

To minimize the effects of lateral variations of conductivity it is convenient, once analyzed the $\rho_{xy}$ and $\rho_{yx}$ sections, to carry out an inversion of the effective values of the apparent resistivity and phase (Berdichevsky and Dmitriv, 1976). The effective impedance is determined according to
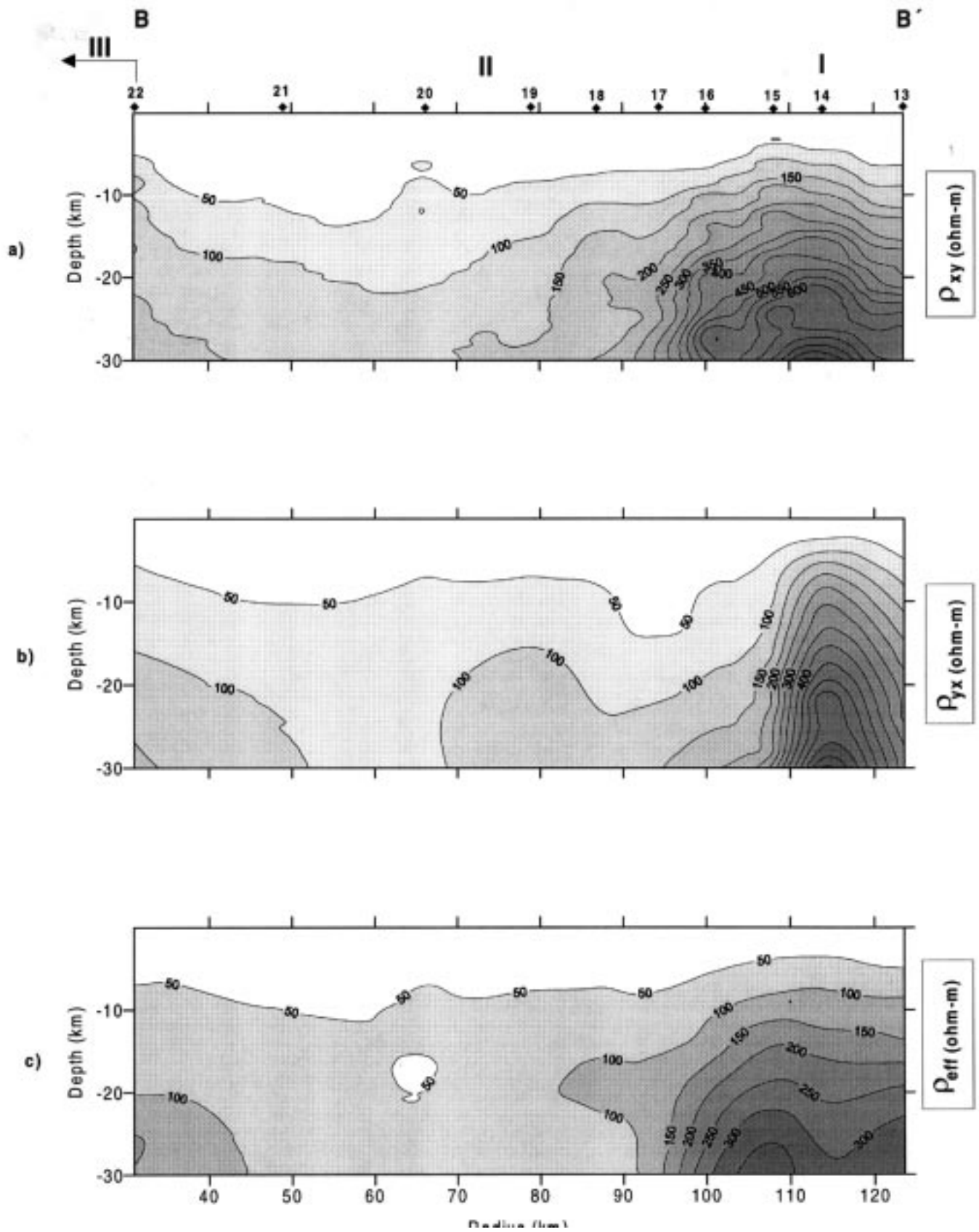
278

Fig. 7. Bostick geoelectric models. a) xy mode, b) yx mode and c) effective mode. I, II and III: gravity characteristic zones.

$$Z_{eff} = \sqrt{(Z_{xx}Z_{yy}) - (Z_{xy}Z_{yx})} \ . \qquad (3)$$

From $Z_{eff}$ we may find $\rho_{eff}(\omega)$ and $\phi_{eff}(\omega)$. Figure 7c shows the results of a Bostick inversion for $\rho_{eff}(\omega)$ and $\phi_{eff}(\omega)$. A good correspondence with the results obtained in models 7a and 7b supports the predominant 1-D character of the studied medium.

## OCCAM INVERSION

Application of Occam algorithm (Constable *et al.,* 1987) leads to a simple model containing the essential properties of all possible models fitting the field data. A large number of geoelectric models could match the observed data, some of which may be very complex. When attempting to achieve a better fit between small portions of the calculated and observed curve of $\rho(\omega)$, $\phi(\omega)$, the complexity of the obtained model increases and the results are often unreliable. The model should be as complex as the medium, but not more complex. The algorithm departs from a half-space and produces a stratified medium. The resistivities vary until an adequate fit between the field and calculated curves is achieved.

Roughness (or the inverse of softness) is defined in terms of the first and the second derivatives of the electric resistivity with respect to the depth as

$$R_1 = \int (dm/dz)^2 \, dz, \qquad \text{or} \qquad (4)$$

$$R_2 = \int (d^2m/dz^2)^2 \, dz \ , \qquad (5)$$

where m (z) is the resistivity or log resistivity, Z is the depth, and $R_1$ and $R_2$ are roughness functions.

The strategy is to find a model that minimizes $R_1$ or $R_2$.

Figure 8 shows the geoelectric sections obtained by stitching together the 1-D models resulting from Occam inversion. The models shown in the Figures 8a, 8b and 8c are very similar to those in Figures 7a, 7b and 7c. This supports our earlier solutions. Thus, in spite of the 1-D character of the studied medium, the differences between the $\rho_{xy}$ and $\rho_{yx}$ models (Figures 7 and 8), as well as the results of the analysis of Tipper and Skew sections (Figure 5), suggest the need to carry out a 2-D inversion of the MT soundings.

A 2-D model may better define a structural model for the crater, particularly between soundings 13 and 16 (Fig-ures 7 and 8), where high values of Tipper and Skew (Figure 5) indicate a more complex structure. It will help to improve the model between soundings 20 to 22 (Figures 7 and 8), where we observe an increase of resistivity with depth.

## CONCLUSIONS

One-dimensional inversion of ten MT soundings was performed in the Yucatán peninsula using the Bostick and Occam inversion schemes. Agreement between both results is found. The geoelectric sections define the structural boundary of the impact structure around sounding 16, with a diameter of approximately 200 km.

High resistivity values ($\rho > 150$ ohm-m) outside of the cenote ring contrasts with lower resistivity values ($\rho < 150$ ohm-m) inside the cenotes ring. This electric characteristic corresponds to the prevalence of little or no fractured rock outside the cenotes ring (beyond 100 km radial distance) and a considerable thickness of highly fractured and porous material for the impact structure filling.

The sub-surface electric resistivity correlates with the Bouguer anomalies. Gravity highs are associated with solid and resistive rocks, while gravity lows agree with increased thicknesses of conductive and fractured filling.

The 1-D approach is adequate in the area, as suggested by similar $\rho_{axy}(\omega)$, $\rho_{ayx}(\omega)$, $\rho_{xy}(z)$, $\rho_{yx}(z)$ and $\rho_{eff}(z)$ profiles. An analysis of the distortion of the magnetotelluric data was carried out from values calculated for Tipper and Skew. The results of this analysis indicated that a 2-D inversion might lead to some significant improvements.
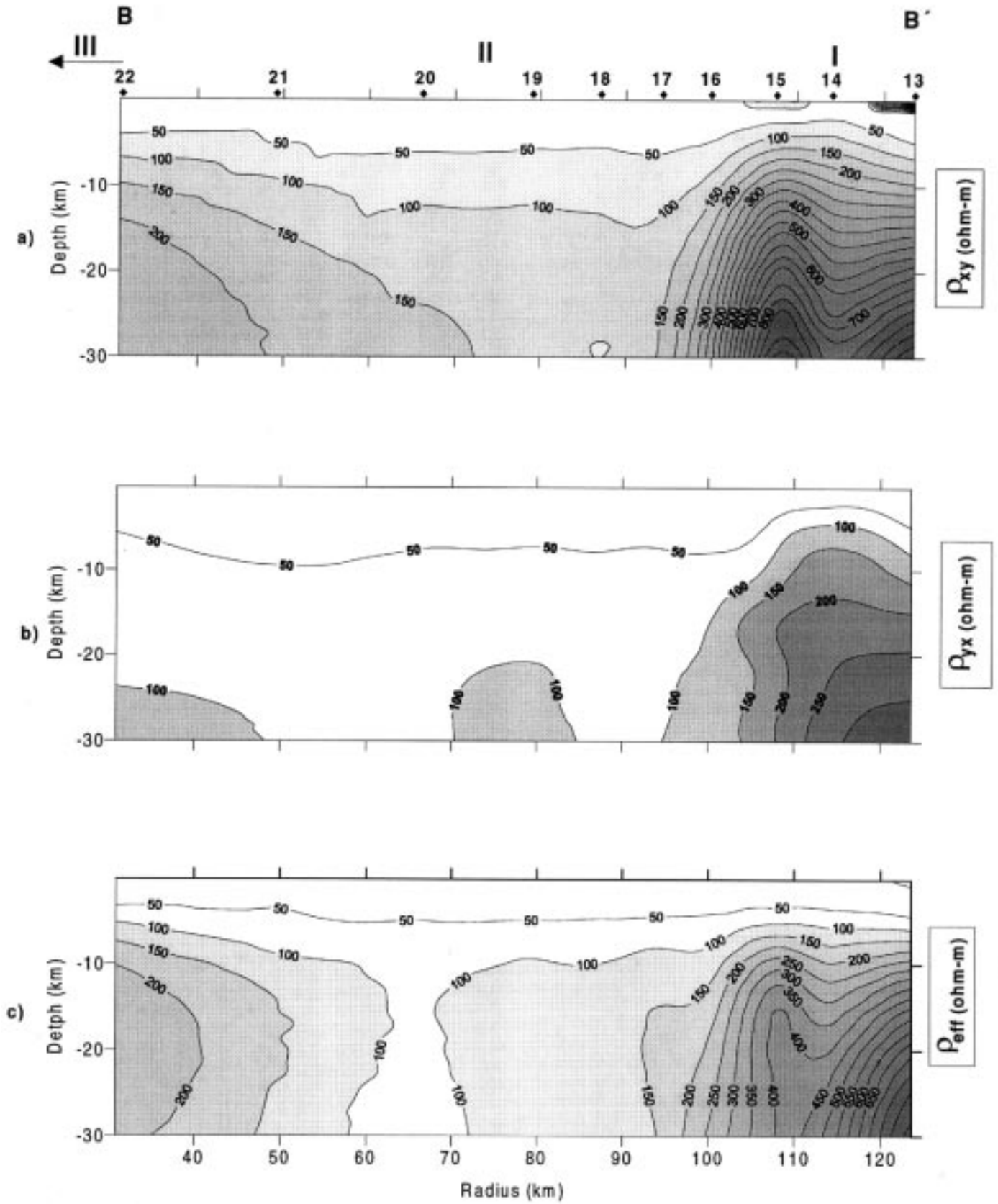
## ACKNOWLEDGMENTS

Fig. 8. Occam geoelectric models. a) xy mode, b) yx mode and c) effective mode. I, II and III: gravity characteristic zones.

## BIBLIOGRAPHY

ALVAREZ, L.W., W. ALVAREZ, F. ASARO and H. MICHEL, 1980. Extraterrestrial cause for the Cretaceous/Tertiary extinction. *Science, 208,* 1095-1108.

BERDICHEVSKY, M. N. and V. I. DMITRIV, 1976. Basic principles of interpretation of magnetotelluric sounding curves. A. Adam (Editor). Geoel. Geoth. Studies. KAPG Geophysycal Monograph. Akademiai Kiado. Budapest, 165-221.

BOSTICK, F. X., 1977. A simple almost exact method of magnetotelluric analysis. *In:* Ward, S., Ed., Workshop of Electrical Methods in Geothermal Exploration, Univ. of Utah Res. Inst., U. S. Geol. Surv. Contract 14-08-0001-g-359.

BOURGEOIS, J., T. A. HANSEN, P. L. WILBERG and E. G. KAUFFMAN, 1988. A tsunami deposit at the Cretaceous-Tertiary boundary. *Science, 241,* 567-570.

CAGNIARD, L., 1953. Basic theory of the magnetotelluric method of geophysical prospecting. *Geophys., 18,* 605-635.

CAMPOS-ENRÍQUEZ, J. O., J. A. ARZATE, J. URRUTIA-FUCUGAUCHI and O. DELGADO-RODRÍGUEZ, 1997. The subsurface structure of the Chicxulub crater (Yucatan, Mexico): Preliminary results of a magnetotelluric study. *The Leading Edge, 16,* 1774-1777.

CONSTABLE, S. C., R. L. PARKER and C. G. CONSTABLE, 1987. Occam's inversion: A practical algorithm for generating smooth models from electromagnetic sounding data. *Geophys., 52,* 289-300.

DELGADO-RODRÍGUEZ, O., J. URRUTIA-FUCUGAUCHI, J. A. ARZATE and J. O. CAMPOS-ENRÍQUEZ, 2001. Coast effect in magnetotelluric soundings on the Yucatan peninsula, Mexico. *Geofís. Int., 40*, 31-41.

ESPÍNDOLA, J. M., M. MENA, M. DE LA FUENTE and J. O. CAMPOS-ENRÍQUEZ, 1995. A model of the Chicxulub impact structure (Yucatan, Mexico) based on its gravity and magnetic signatures. *Phys. Earth Plant. Inter., 92,* 271-278.

HENKEL, H., 1992. Geophysical aspects of meteorite impact craters in eroded shield environment, with special emphasis on electrical resistivity. *Tectonophys., 216,* 63-89.

HILDEBRAND, A. R., G. T. PENFIELD, D. A. KRING, M. PILKINGTON, A CAMARGO, S. JACOBSEN and W. BOYTON, 1991. Chicxulub crater: A possible Cretaceous/Tertiary boundary impact crater on the Yucatan Peninsula, Mexico. *Geology, 19,* 867-871.

HILDEBRAND, A. R., M. PILKINGTON, C. ORTÍZ-ALEMÁN, R.E. CHÁVEZ, J. URRUTIA-FUCUGAUCHI, M. CONNORS, E. GRANIEL, A. CAMARA, J. F. HALPENNY and D. NIEHAUS, 1998. Mapping Chicxulub crater structure with gravity and seismic reflection data. *In:* Grady, M.M. *et al.* (Eds.), Meteorites: Flux with Time and Impact Effects, Geol. Soc., London, Sp. Publ., 140, 155-176.

KELLET, R. L., F. E. M. LILLEY and A. WHITE, 1991. A two-dimensional interpretation of the geomagnetic coast effect of southeast Australia, observed on land and seafloor. *Tectonophys., 192,* 367-382.

MORGAN, J. and M. WARNER,1999. Morphology of the Chicxulub impact: Peak-ring crater or multi-ring basin? *In:* Dressler, B.O. and Sharpton, V.L. (Eds.), Large Meteorite Impacts and Planetary Evolution, Geol. Soc. Am. Sp. Paper, 339, 281-290.

MORGAN, J., M. WARNER and CHICXULUB WORKING GROUP, 1997. Size and morphology of the Chicxulub impact crater. *Nature, 390,* 472-476.

PARKINSON, W. D., 1959. Directions of rapid geomagnetic fluctuations. *Geophys. J. R. Astron. Soc., 2,* 1-14.

PENFIELD, G. T. and Z. A. CAMARGO, 1981. Definition of a major igneous zone in the central Yucatan platform with aeromagnetics and gravity. 51st Ann. Internat. Mtg. SEG, Abstract,. 37.

PILKINGTON, M. and R. GRIEVE, 1992. The geophysical signature of terrestrial impact craters. *Rev. Geophys., 30,* 161-181.

PILKINGTON, M., A. R. HILDEBRAND and C. ORTÍZ-ALEMÁN, 1994. Gravity and magnetic field modeling and structure of the Chicxulub crater, Mexico. *J. Geophys. Res., 99,* 147-162.

REBOLLEDO-VIEYRA, M., J. URRUTIA-FUCUGAUCHI, L. MARÍN, A. TREJO-GARCÍA, V. L. SHARPTON and A. M. SOLER-ARECHALDE, 2000. UNAM scientific shallow drilling program of the Chicxulub impact crater. *Int. Geol. Rev., 42,* 928-940.

SHARPTON, V. L., G. B. DALRYMPLE, L. MARÍN, B. C. RYDER, B. C. SCHUARAYTZ and J. URRUTIA-FUCUGAUCHI, 1992. New links between the Chicxulub impact structure and the Cretaceous/Tertiary boundary. *Nature, 359,* 819-821.

SHARPTON, V. L., K. BURKE, A. CAMARGO, S. A. HALL, D. SCOTT-LEE, L. MARIN, G. SUÁREZ, J. M. QUEZADA, P. D. SPUDIS and J. URRUTIA-FUCUGAUCHI, 1993. Chicxulub multiring impact basin: Size and other characteristics derived from gravity analysis. *Science, 261,* 1564-1567.

SNYDER, D. B., R. W. HOBBS and CHICXULUB WORKING GROUP, 1999. Deep seismic reflection profiles across the Chicxulub crater. *In:* Dressler, B. O. and Sharpton, V. L. (Eds.), Large Meteorite Impacts and Planetary Evolution, Geol. Soc. Am. Sp. Paper, 339, 263-268.

URRUTIA-FUCUGAUCHI, J., L. MARIN and A. TREJO-GARCÍA, 1996. UNAM scientific drilling program of the Chicxulub impact structure – evidence for a 300 km crater diameter. *Geophys. Res. Lett., 23,* 1565-1568.

VOZOFF, K., 1989. The magnetotelluric method. *In:* Nabigian, M. N. (Ed.), Electromagnetic Methods in Applied Geophysics, Soc. Expl. Geophys. Tulsa, OK, USA.

---

Omar Delgado-Rodríguez[1,*], Oscar Campos-Enríquez[1], Jaime Urrutia-Fucugauchi[1] and Jorge A. Arzate[2]

[1] *Laboratorio de Paleomagnetismo y Geofísica Nuclear, Instituto de Geofísica. Universidad Nacional Autónoma de México, Del. Coyoacán 04510 México D.F., MÉXICO*

[*] *Now at Instituto Mexicano del Petróleo. Eje Central Lázaro Cárdenas 152. Atepehuacan, 07730 México D.F., MÉXICO Email: odelgado@imp.mx*

[2] *Unidad de Investigación en Ciencias de la Tierra, Instituto de Geofísica, Universidad Nacional Autónoma de México, Campus Juriquilla, Querétaro, MÉXICO*